NANO EXPRESS

Effects of Anisotropy and In-Plane Grain Boundary in Cu/Pd Multilayered Films with Cube-on-Cube and Twinned Interface

Xiang Chen[1,2], Shayuan Weng[1,2], Xing Yue[1,2], Tao Fu[1,2*] and Xianghe Peng[1,2,3*]

Abstract

In crystalline materials, grain boundary and anisotropy of crystal structure affect their mechanical properties. The effects of interfacial structure on the mechanical properties may be diverse when the multilayer film is loaded along different directions. In this work, we performed a series of molecular dynamics simulations of the tension of in-plane single and polycrystalline Cu/Pd multilayered films with cube-on-cube (COC) and twinned interfaces to explore the effects of the interfacial structure, loading direction and in-plane grain boundaries on their mechanical properties. The interfacial misfit dislocation lines become bent after relaxation, and the high temperature of 300 K was found as a necessary condition. When stretched along ⟨110⟩ direction, the strengthening effect of the COC interface is more noticeable; however, when stretched along ⟨112⟩ direction, the twin interface's strengthening effect is more visible, showing the anisotropic effect of interfacial structure on mechanical properties. However, in the in-plane honeycomb polycrystalline sample, the twin interface showed a pronounced strengthening effect, and no jogged dislocations were observed.

Keywords: Interfacial structure, Anisotropy of mechanical properties, Strengthening effect, In-plane polycrystalline

Introduction

Nanostructured metallic multilayered (NMM) films have attracted much attention due to their excellent mechanical properties [1–3], which are usually superior to their constituents. The interface, transition zone between different individual layers, is one of the most common planar defects in NMM films, which can act as sources and sinks of defects via absorption and annihilation, barriers and storage sites for defects [4–7].

The interfaces in an NMM film can be divided into a coherent, semi-coherent and non-coherent interface based on the lattice mismatch between their constituents on both sides of the interface [4]. Copper-palladium (Cu/Pd) and gold–nickel (Au/Ni) multilayered films are

the earliest found multilayered films possessing excellent mechanical properties[8]. Yang et al. measured the biaxial elastic modulus Y[111] of Cu/Pd and Au/Ni multilayered films by bulge testing and found their biaxial elastic modulus increases drastically from 0.27 to 1.31 TPa and from 0.21 to 0.46 TPa, respectively [8]. Subsequently, Davis et al. used more advanced techniques to measure elastic and structural properties of Cu/Pd and Cu/Ni multilayered films with the same growth textures and composition modulation amplitudes [9, 10]. However, no significant anomalous elastic behavior has been observed [9, 10], which raises whether the supermodulus effect exists in the Cu/Pd multilayers. The mechanical properties of NMM are strongly dependent on the interfacial structure between adjacent individual layers [11]. Howe et al. investigated the interfacial structure of Pd films on Cu(111) and found that the Pd grows in a twinned FCC structure along ⟨111⟩ direction [12]. The twinning

*Correspondence: futaocqu@163.com; futao@cqu.edu.cn; xhpeng@cqu.edu.cn
[1] College of Mechanical Engineering, Chongqing University, Chongqing 400044, China
Full list of author information is available at the end of the article

Chen *et al. Nanoscale Res Lett*   (2021) 16:69

Page 2 of 10

structures at the interface usually have a profound effect on their strength [11].

Weng et al. investigated the effect of interfacial structure on the deformation behaviors of Cu/Ni multilayered films with coherent, semi-coherent and coherent twin interfaces using molecular dynamics (MD) simulation and found that the coherent twin interface shows significant strengthening [7]. However, in our recent work, the inapparent strengthening effect of the twin interface in Cu/Pd multilayered films was observed under tension along $\langle 110 \rangle$ direction [13]. Besides, the shape of the misfit dislocation network would change during energy minimization and relaxation. Shao et al. investigated the relaxation mechanisms of interfaces and the evolution of interfacial dislocation networks in the Cu/Ni multilayered films by MD simulations [14–17]. These works' loading direction is often perpendicular to the interface, referred to as out-of-plane [7, 18, 19]. However, the interface may play different roles during loading along different directions due to the anisotropy of the mechanical properties of crystals [20–23].

Besides, multilayered films are more inclined to be subjected to the load parallel to the interface in practice, referred to as in-plane loading. Zhou et al. proposed a strengthening mechanism governed by multiple necklace-like extended jogged dislocations in a columnar-grained nano-twinned metal subjected to external stress paralleled to the twin planes [20], which is also observed in Cu/Ni multilayer [21]. These jogged dislocations are rarely found in a simulation under an out-of-plane loading [7, 18, 19, 24]. In available MD simulations of in-plane tensions, the sample is usually stretched along a specific direction, i.e., $\langle 112 \rangle$ or $\langle 110 \rangle$ direction [25]. However, few comparative studies under tension along these two directions have been conducted. On the other hand, the individual layer of the multilayered film prepared by experiments is usually in-plane polycrystalline containing many grain boundaries (GBs) perpendicular to the interface.

The jogged dislocations mentioned above are often observed in the coherent twined films or twined multilayered films with a minor mismatch. Whether these jog dislocations can form in a twin interface film with a high mismatch is still unknown. The Cu/Pd multilayered film is the earliest found multilayered film having excellent mechanical properties [8, 12, 26–28]. Its lattice mismatch (~7.07%) is larger than that of Cu/Ni multilayered films (~2.7%). Therefore, the strengthening and weakening mechanism [7, 14–17] obtained by the Cu/Ni multilayered film may not be applied to the Cu/Pd multilayered film. Two common interfaces [3], twin and cube-on-cube interface, are observed in Cu/Pd multilayered film by experimental characterization [12]. Understanding the effect of interfacial structure on multilayered films' mechanical properties would be significant for designing high-performance nano-multilayer films with a large lattice mismatch.

In this work, two types of samples with in-plane honeycomb crystal and single-crystal are developed. For each type of sample, two kinds of interfaces (cube-on-cube and twin) are considered. Then we perform a series of MD tension simulations of these Cu/Pd multilayered films to explore the effects of the interfacial structure, loading direction, and in-plane GBs on their mechanical properties.
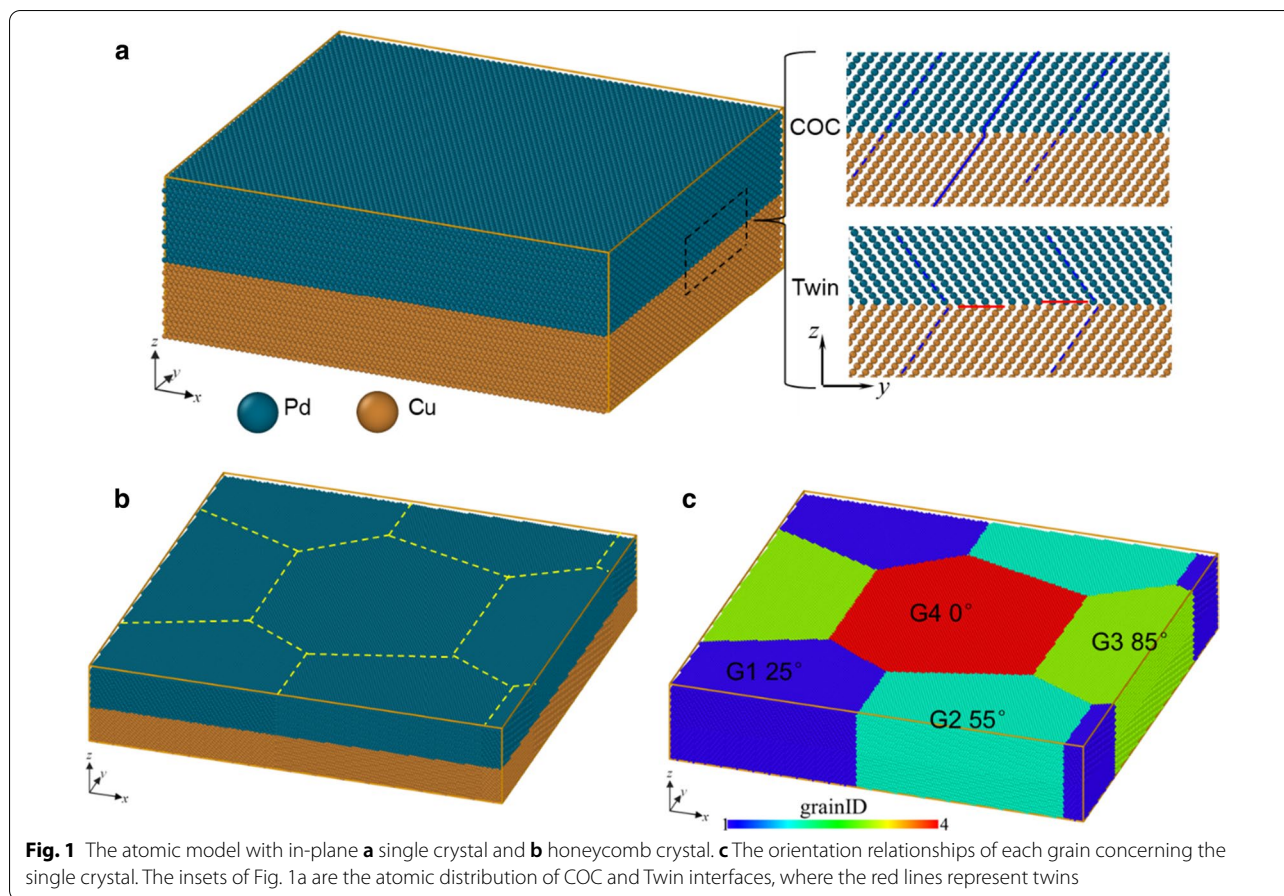
Methods

Three sets of parameters for Cu–Cu, Pd–Pd, and Cu–Pd are needed to be identified, respectively. We choose the second nearest-neighbor modified embedded atom method (2NN MEAM) potential [29, 30] to describe the interactions between atoms. For the Cu–Cu and Pd–Pd, their potential parameters have been developed by Lee et al. [31]. Based on the single elements' potential parameters, we fitted a set of Cu–Pd binary potential parameters in our previous work [26], as listed in Table 1. These parameters can reproduce the fundamental physical and mechanical properties of pure Cu, Pd and their alloys and describe the formation mechanism of growth twins [26].

The FCC/FCC multilayered film is prone to grow along $\langle 111 \rangle$ directions and the orientation relationship of the interface is identified as $\{111\}_{FCC}/\{111\}_{FCC}$ [32, 33]. Therefore, we only consider the Cu{111}/Pd{111} interfaces in this work. Two types of samples with in-plane single crystal (SC) and honeycomb crystal (HC) are built, as shown in Fig. 1a and b. For each type of sample, cube-on-cube (COC) and twin interface are considered. Therefore, four samples are built, named SC COC, SC Twin, HC COC and HC Twin. For SC COC, the crystal orientations of the Cu layer and the Pd layer are identical;

Table 1 2NN MEAM potential parameters for the Cu-Pd system [26]. E_c, r_e, and B are cohesive energy, equilibrium nearest-neighbor distance and bulk modulus of B2 CuPd alloy

Parameter	E_c (eV)	r_e (Å)	$_B$ (GPA)	d	Cu–Pd–Cu		Pd–Cu–Pd		Cu–Cu–Pd		Pd–Pd–Cu	
					C_{min}	C_{max}	C_{min}	C_{max}	C_{min}	C_{max}	C_{min}	C_{max}
Value	3.725	2.593	106.2	0.05	0.65	1.44	0.78	1.44	1.44	2.8	1.44	2.8

Chen *et al. Nanoscale Res Lett*   (2021) 16:69

Page 3 of 10

Fig. 1 The atomic model with in-plane **a** single crystal and **b** honeycomb crystal. **c** The orientation relationships of each grain concerning the single crystal. The insets of Fig. 1a are the atomic distribution of COC and Twin interfaces, where the red lines represent twins

however, for SC Twin, their crystal orientations are symmetric about the twin interface, as shown in the inset of Fig. 1a. The orientation relations and dimensions of each direction are listed in Table 2.

The in-plane honeycomb sample is built using the Voronoi construction method with the in-plane single crystal as a representative unit, as shown in Fig. 1b. In HC samples, there are four grains, whose orientation relationships concerning the single crystal (Fig. 1a) are counterclockwise rotation of 25°, 55°, 85° and 0° about the z-axis, respectively. The sizes of HC COC and HC Twin are listed in Table 2.

The energy minimization is firstly used to optimize the interfacial structure at 0 K. Then, the relaxation is performed on each sample under the isothermal-isobaric (NPT) ensemble [34, 35] at 300 K for 20 ps to achieve

Table 2 Crystal orientations and sizes of each direction of samples. a_{Cu} and a_{Pd} are the lattice parameters of Cu and Pd (3.615 Å and 3.890 Å)

In-plane	Sample	Constituent	l_x	l_y	l_z	Model
Single-crystal (SC)	COC	Pd layer	$80 \times \frac{1}{2}[01\bar{1}]a_{Pd}$	$40 \times \frac{1}{2}[\bar{2}11]a_{Pd}$	$18 \times \frac{1}{3}[111]a_{Pd}$	SC COC
		Cu layer	$86 \times \frac{1}{2}[01\bar{1}]a_{Cu}$	$43 \times \frac{1}{2}[\bar{2}11]a_{Cu}$	$18 \times \frac{1}{3}[111]a_{Cu}$	
	Twin	Pd layer	$80 \times \frac{1}{2}[01\bar{1}]a_{Pd}$	$40 \times \frac{1}{2}[\bar{2}11]a_{Pd}$	$18 \times \frac{1}{3}[\bar{1}\bar{1}\bar{1}]a_{Pd}$	SC Twin
		Cu layer	$86 \times \frac{1}{2}[01\bar{1}]a_{Cu}$	$43 \times \frac{1}{2}[\bar{2}11]a_{Cu}$	$18 \times \frac{1}{3}[111]a_{Cu}$	
Honeycomb crystal (HC)	COC	Pd layer	400 Å	400 Å	$18 \times \frac{1}{3}[111]a_{Pd}$	HC COC
		Cu layer	400 Å	400 Å	$18 \times \frac{1}{3}[111]a_{Cu}$	
	Twin	Pd layer	400 Å	400 Å	$18 \times \frac{1}{3}[\bar{1}\bar{1}\bar{1}]a_{Pd}$	HC Twin
		Cu layer	400 Å	400 Å	$18 \times \frac{1}{3}[111]a_{Cu}$	

Chen *et al. Nanoscale Res Lett* (2021) 16:69

Page 4 of 10

an equilibrium system with zero pressure in *x-*, *y-* and *z-* directions. Uniaxial tension simulations of SC COC and SC Twin along different directions (*x-* or *y-*) with a strain rate of 5×10^8 s^{-1} are performed with the Large-scale Atomic/Molecular Massively Parallel Simulator (LAMMPS) [36]. We also perform tensile simulations of HC COC and HC Twin to study the effects of in-plane GBs and the interfacial structures on their mechanical properties. During loading, the pressures in the other two directions are kept at zero to satisfy the requirement of uniaxial tensile deformation. In all simulations, periodic boundary conditions are applied along the *x-*, *y-* and *z-*directions.

We choose the dislocation extraction algorithm (DXA) [37] to analyze local structures, using which the atoms can be divided into different types (FCC, BCC, HCP, etc.) based on their local structures. It can identify the common dislocations in FCC crystal and determine their Burgers vectors and output dislocation lines [37]. The atoms are colored as the following rule: green for FCC, red for HCP, blue for BCC and white for "other" local crystal structures. It is known that both stacking faults (SFs) and twin boundaries/interfaces (TBs/TIs) are identified as HCP structures, and two adjacent red

atomic layers and the single red atomic layer are SF and TB/TI, respectively. An open-source visualization software, OVITO [38], is used to visualize the evolution of microstructures.

Results and Discussion

Characterization of interfacial structures

Figure 2 shows the interfacial atomic configuration in SC COC and SC Twin after energy minimization and relaxation, where the atoms identified as FCC have been removed for clarity. From Fig. 2, we can see that the interface mismatch dislocation network is triangular in periodicity, which is consistent with that in the Ag(111)/Ni(111) multilayered film [39]. The difference is that the interface in SC COC is composed of alternating coherent regions (CRs) and SF regions. In contrast, the interface in SC Twin is entirely composed of TBs. These TBs are at adjacent atomic layers and are composed of Cu and Pd atoms alternate in adjacent triangles, which can also be confirmed by the height of the two red solid lines (represent the TBs) in the inset of Fig. 1a. During the energy minimization, the potential energy of the system is minimized by the slight movement of atoms, and the size of samples in each direction cannot change freely. In this
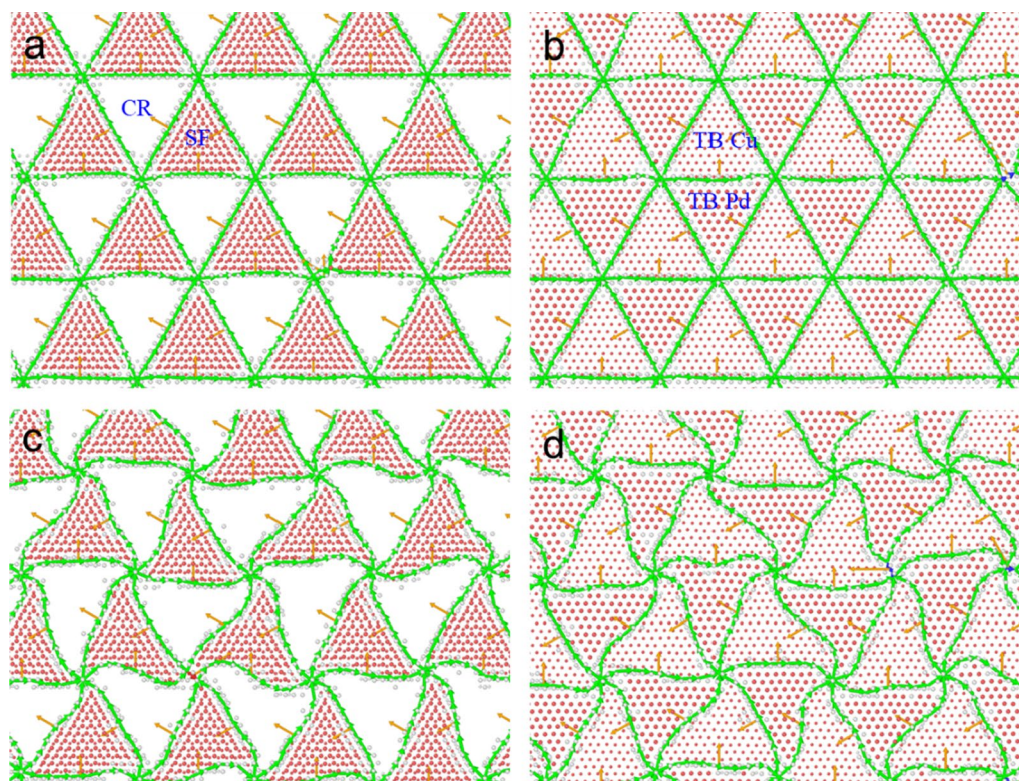

Fig. 2 Interfacial atomic configuration after energy minimization: **a** SC COC, **b** SC Twin, and after relaxation: **c** SC COC, **d** SC Twin. The large and small atomic balls represent Pd and Cu, respectively. The atoms identified as FCC have been removed for clarity

stage, it is mainly to optimize the local structure, specifically, the interfacial structure. Hence, the dislocation lines remain straight after the energy minimization, as shown in Fig. 2a and b. During the energy minimization, the sample size is fixed, which would induce the residual stresses in all directions. These residual stresses cannot be loosed sufficiently after energy minimization.

During the relaxation, the sample size allows changing to relax the residual stress to zero pressure in all directions. After relaxation, the misfit dislocation lines become bent (Fig. 2c, d). This phenomenon of the misfit dislocation network can also be found in the semi-coherent Cu{111}/Ni{111} interface [40, 41]. By comparing the number of atoms with different local structures, especially HCP, we can find that the number of atoms in different lattice structures changes insignificantly, indicating that the total area of SF and TB varies insignificantly.

To explore whether the temperature is a necessary condition for the bending of dislocation lines, the samples after minimization are relaxed at a low temperature of 10 K for comparison and find that the dislocation lines remain straight. Therefore, a higher temperature is a necessary condition to cause the bending of the dislocation line. Specifically, due to the increased thermal activation at high temperatures, the atoms around the dislocation lines can overturn the energy barrier to move from one atomic column to the adjacent densely packed atomic column. Therefore, the bending magnitude of the dislocation is only one to two atomic layer distances. Similar bending of the dislocation line in the dislocation network can also be observed in the samples with in-plane honeycomb crystals (HC COC and HC Twin).

Effects of loading direction

Figure 3 shows the stress−strain (σ-ε) curves of SC COC and SC Twin under tension along different directions at a strain rate of 5×10^8 s^{-1}, where one can see that all these curves grow linearly to the highest point, then drop rapidly to a certain value and fluctuate around them. The young's modulus E is obtained by fitting the curves' slope in a strain range of 0.00–0.03, as listed in Table 3. We can see that E along $y\,[\bar{2}11]$ (145.62 GPa for SC COC and 142.95 for SC Twin) is larger than those along $x\,[01\bar{1}]$ (135.04 GPa for COC and 133.84 GPa for Twin). The Es along the same direction but with different interfacial structures are almost identical, showing an insignificant dependence of Es on interfacial structures involved in this work, which is consistent with the experimental results of Cu-Co [42], Cu/Pd and Cu/Ni [9] multilayered films.

In a cubic material, the elastic moduli along any orientation can be determined from the elastic constants by application of the following equation [22]:
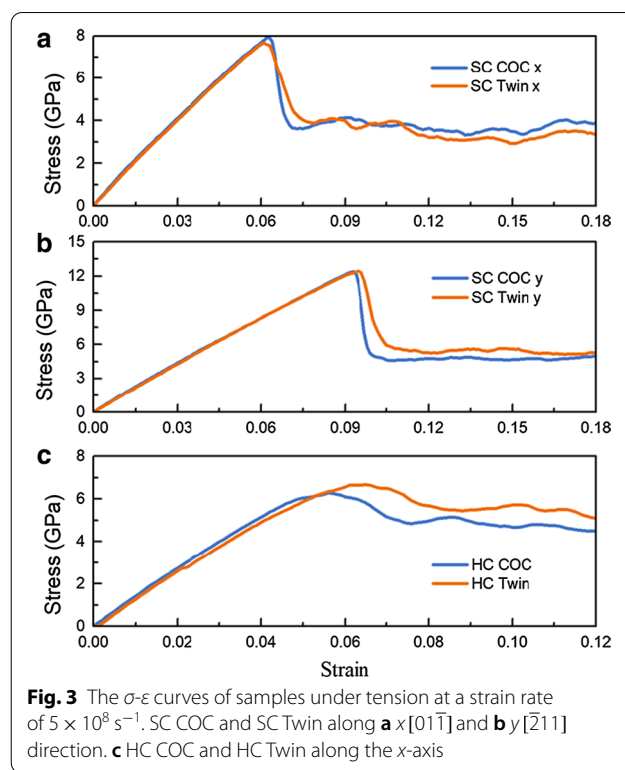

Fig. 3 The σ-ε curves of samples under tension at a strain rate of 5×10^8 s^{-1}. SC COC and SC Twin along **a** $x\,[01\bar{1}]$ and **b** $y\,[\bar{2}11]$ direction. **c** HC COC and HC Twin along the x-axis

Table 3 E, σ_m, ε_m, and σ_f of samples under tension along x- or y-direction at a strain rate of 5×10^8 s^{-1}

	Loading direction	E (GPa)	σ_m (GPa)	ε_m	σ_f (GPa)
SC COC	$x\,[01\bar{1}]$	135.04	7.93	0.063	3.500.08
SC Twin	$x\,[01\bar{1}]$	133.84	7.66	0.061	3.110.07
SC COC	$y\,[\bar{2}11]$	145.62	12.39	0.093	4.760.07
SC Twin	$y\,[\bar{2}11]$	142.95	12.42	0.095	5.500.12
HC COC	x	137.38	6.27	0.056	4.920.16
HC Twin		136.08	6.66	0.065	5.550.08

$$
\frac{1}{E_{ijk}} = S_{11} - 2\left(S_{11} - S_{12} - \frac{1}{2}S_{44}\right)
$$
$$
\times \left(l_{i1}^2 l_{j2}^2 + l_{j2}^2 l_{k3}^2 + l_{i1}^2 l_{k3}^2\right),
\tag{1}
$$

where S_{11}, $S_{12,}$ and S_{44} are elastic compliance constants; E_{ijk} is Young's modulus in the $[ijk]$ direction; l_{i1}, l_{j2} and l_{k3} are the cosines of the direction $[ijk]$. However, the coefficients about the crystal direction $\left(l_{i1}^2 l_{j2}^2 + l_{j2}^2 l_{k3}^2 + l_{i1}^2 l_{k3}^2\right)$ in Eq. (1) along $\langle 112 \rangle$ and $\langle 110 \rangle$ directions are identical (0.25), therefore, for Cu and Pd, $E_{\langle 112 \rangle} = E_{\langle 110 \rangle}$. When the deformation is parallel to the interface, the mixing rule, $E_{[ijk]}^{\mathrm{Cu/Pd}} = E_{[ijk]}^{\mathrm{Cu}} f_{\mathrm{Cu}} + E_{[ijk]}^{\mathrm{Pd}} f_{\mathrm{Pd}}$, can be used to calculate E. f_{Cu} and f_{Pd} are the volume fraction of Cu and Pd,

Chen *et al. Nanoscale Res Lett*   (2021) 16:69

Page 6 of 10

respectively, and $f_{Cu} + f_{Pd} = 1$. In this work, f_{Cu} and f_{Pd} are invariant for samples with different interfaces. Therefore, $E_{\langle 112 \rangle}^{Cu/Pd}$ should be equal to $E_{\langle 110 \rangle}^{Cu/Pd}$. However, the *E*s along $\langle 110 \rangle$ and $\langle 112 \rangle$ are different, which should be attributed to the elastic anisotropy of the interface-affected zone [6, 42].

The maximum stress (σ_m) obtained by tension along *y*-axis is larger than that along *x*-axis for both COC and Twin interface, which should be ascribed to the Schmidt factor μ. The σ_m of the curve corresponds to the nucleation of dislocation [43–45]. $\mu = \cos\phi\cos\lambda$, where ϕ and λ are the Angle between the tensile direction and the normal direction of the slip plane and the Angle between the tensile direction and the slip direction, respectively. Moreover, when the tension is along x [01$\bar{1}$], the σ_m and corresponding strain ε_m of SC COC is slightly higher than that of the SC Twin, which is consistent with the work by Weng et al. [25]. However, when the tension is along y [$\bar{2}$11], the σ_m and ε_m of SC COC are slightly lower than that of SC Twin. We further perform additional MD simulations at a lower strain rate of 1×10^8 s^{-1} and obtained similar results. However, overall, the difference between them is slight and can be almost ignored.

After the stress reaches the highest point, many dislocations nucleate successively to release the stored elastic potential energy, causing the rapid drop of stress [46]. The interaction between dislocations, the interaction between dislocations and interface, and the nucleation of new dislocations are the primary mechanism at the flow-stress stage. The σ_f is the average stress in $0.121 < \varepsilon < 0.150$, as listed in Table 3. Unlike the tiny difference in E, σ_m and ε_m, the difference between the σ_f for the different interfacial structures is significant. When the tension is along x [01$\bar{1}$], the σ_f of SC COC is larger than that of SC Twin, showing the strengthening effect of the COC interface is more obvious than that of the Twin interface, which is consistent with the work by Weng et al. [25]. However, when the tension is along y [$\bar{2}$11], the σ_f of SC Twin is 15.55% larger than that of SC COC, showing an obvious strengthening of the twin interface, which accords with the traditional cognition of strengthening effect of twin boundary. The comparison of flow stress in these two directions shows that the strengthening effect of the interfacial structure depends on the loading direction. In the flowing section, we will examine the mechanical response of in-plane honeycomb crystal samples.

Effects of in-plane GBs

We further perform MD tension simulation of HC COC and HC Twin at a strain rate of 5×10^8 s^{-1}, and the σ-ε curve is shown in Fig. 3c. Similarly, we can get E, σ_m, ε_m, and σ_f, as listed in Table 3. Note that E is obtained by fitting the slope of σ-ε curves of HC COC and HC Twin

in a strain range of 0.0–0.02, and σ_f is the average stress in $0.081 < \varepsilon < 0.100$. For HC COC and HC Twin, the *E*s are close and lie between that of SC sample long the *x* [01$\bar{1}$] and *y* [$\bar{2}$11]. The *E*s are slightly larger than those by experiment (115–125 GPa)[9], which should be ascribed to the idealized atomic samples used in this work without taking the additional defects such as vacancies and impurities. Their σ_m is lower than that of the SC sample, which can be ascribed to that the dislocations are easier to nucleate induced by local stress concentration with the introduction of in-plane GBs. Taking the twin interface as an example, Fig. 4 shows the microstructure of the dislocation nucleation location after the stress reaches the highest point, where one can see that in HC Twin, the dislocation nucleates from the junction of the GB and twin interface (Fig. 4a), while in SC Twin samples, the dislocation nucleates from the twin interface both stretched along *x* [01$\bar{1}$](Fig. 4b) and *y* [$\bar{2}$11] (Fig. 4c).

Although the σ_m of the HC sample is lower than those of the SC sample, the σ_f of the HC sample is higher than the SC sample, indicating the strengthening effect of in-plane GBs. This strengthening mainly comes from the following aspects: (1) The in-plane GBs provides more nucleation points for dislocations resulting in more dislocations nucleated, and these dislocations are hindered by the COC and Twin interface; (2) In-plane GBs hinder dislocations. Moreover, σ_f of HC Twin is higher than those of HC COC, which shows that the strengthening effects of dislocation hindered by twin interface are more evident than those by COC interface.

Figure 5 shows the microstructure of HC Twin at the plastic flow stage. It should be noted that during the loading, the nucleation and slip of partial dislocations forming SFs, the movement of these dislocations and SFs limited by the interface inducing hairpin-like partial dislocation glide and the mutual reactions of partial dislocations forming stair-rod dislocation are the primary deformation mechanism. No necklace-like multiple jogged dislocations are observed, which are often observed in Cu/Ni multilayered film [21] and nano-twinned Cu [20] under in-plane tension. It is mainly due to the large lattice mismatch of the Cu/Pd multilayered film with a more complicated interface structure (Fig. 2).

Compared with single-crystal materials, the mechanical properties of polycrystalline samples are often more dependent on the strain rate. Therefore, we perform more MD simulations of tension for HC samples (HC COC and HC Twin) along *x*-direction and SC Twin along *x*- and *y*-directions using a strain rate varied from 5×10^7 s^{-1} to 5×10^9 s^{-1}. The σ-ε curves are shown in Fig. 6a and b, where one can see that the stress increases linearly to the highest point and then decreases. For the HC samples, the stress fluctuates with the increase of
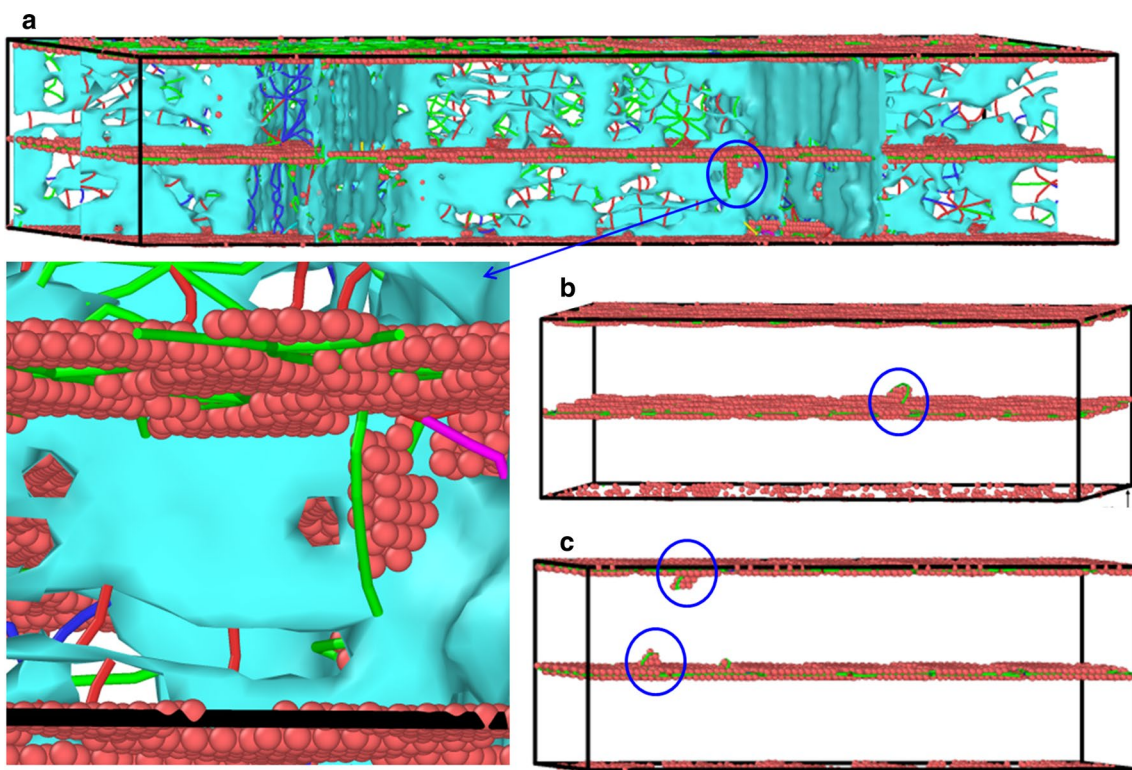
Fig. 4 The microstructure of the dislocation nucleation location after the stress reaches the highest point. **a** HC Twin, SC Twin under tension along **b** x[01$\bar{1}$], **c** y[$\bar{2}$11]
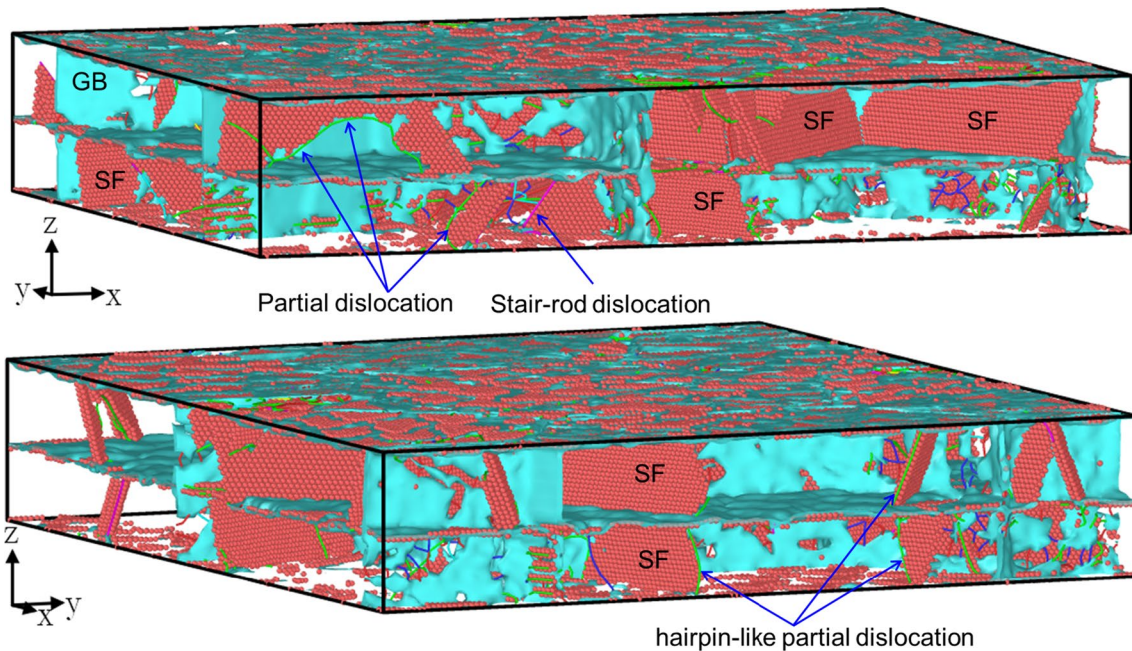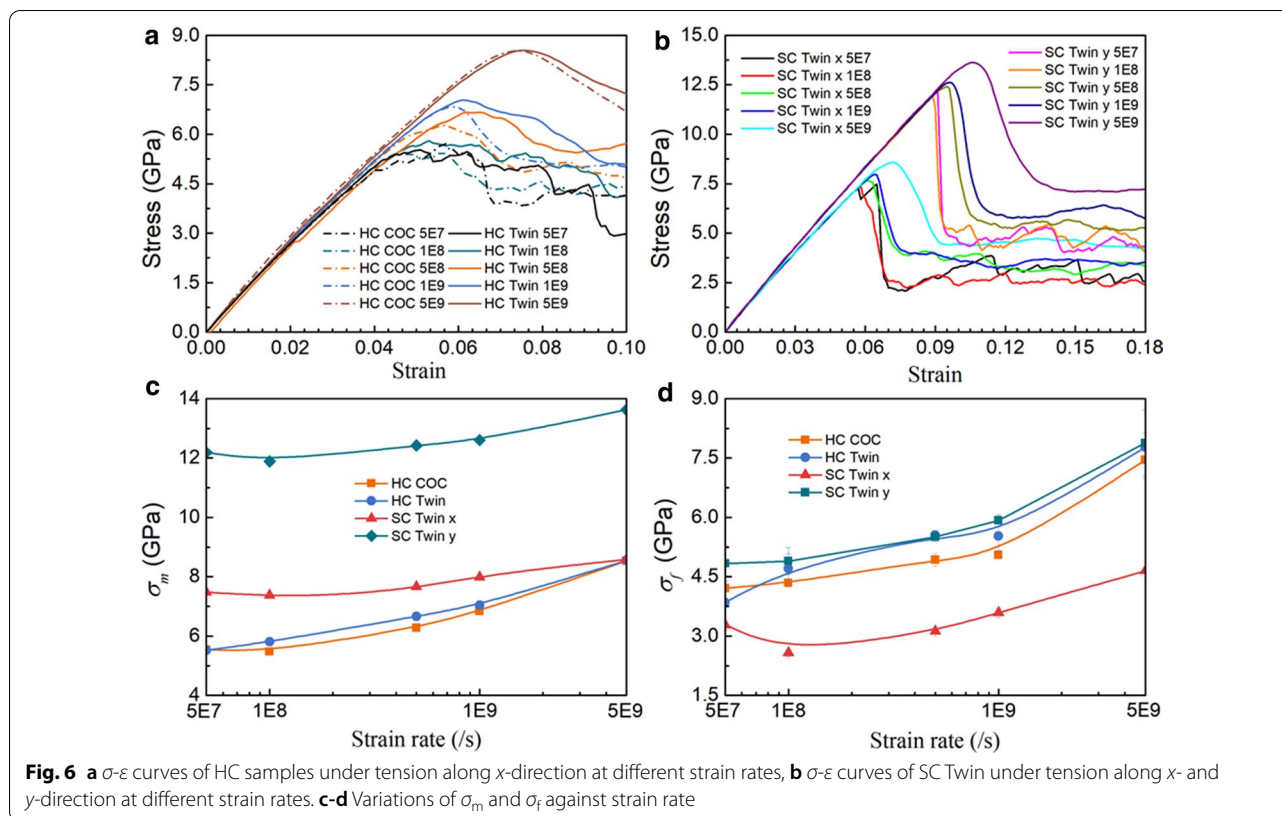

Fig. 5 The microstructure of HC Twin at the plastic flow stage

Chen *et al. Nanoscale Res Lett*   (2021) 16:69

Page 8 of 10

Fig. 6 a σ-ε curves of HC samples under tension along *x*-direction at different strain rates, **b** σ-ε curves of SC Twin under tension along *x*- and *y*-direction at different strain rates. **c-d** Variations of σ_m and σ_f against strain rate

strain at low strain rate in the descending stage, while the stress fluctuation is not apparent at a high strain rate (Fig. 6a and b). Figure 6c and d shows the variations of σ_m and σ_f against strain rate, where σ_m and σ_f increase with increasing strain rate. The σ_m of SC Twin along *y*-direction is much larger than that of other samples, which should be ascribed to the Schmidt factor μ mentioned above. However, due to the strengthening effect of the in-plane grain boundary, the σ_f of HC samples are closed to that of SC Twin along *y* direction. Moreover, σ_f of the samples with the twinned interface are higher than those with the COC interface at high strain rate (1×10^8 s^{-1} to 5×10^9 s^{-1}), indicating the strengthening effect of the twinned interface, but as the strain rate increases, this strengthening effect weakens. It should be noted that at the strain rate of 5×10^7 s^{-1}, the σ_f of HC Twin is lower than that of HC COC, which may be ascribed to the fact that the number of dislocations nucleated at low strain rate is less inducing the weaken strengthening effect of twin interface.

Conclusions

In this work, molecular dynamics tension simulations of in-plane single and polycrystalline Cu/Pd multilayered films with COC and twinned interfaces were performed along various directions to explore the effects of the interfacial structure, loading direction and in-plane grain boundaries on the mechanical properties. We found that the interfacial misfit dislocations present a triangular network structure, and the misfit dislocations lines bend after relaxation. The high temperature of 300 K was a necessary condition for the bending of the dislocation line. The elastic modulus of the sample has no obvious dependence on the interface structure, but it is related to the loading direction. The strengthening effect of the COC interface is noticeable when stretched along the ⟨110⟩ direction; however, the strengthening effect of the twin interface is visible, when stretched along the ⟨112⟩ direction, showing the anisotropic effect of interfacial structure on mechanical properties. Finally, in the in-plane honeycomb polycrystalline model, the twin interface showed a pronounced strengthening effect, and no jogged dislocations were observed.

Chen *et al. Nanoscale Res Lett*   (2021) 16:69

Page 9 of 10

Authors' contributions
XC, SW and TF designed the scheme and wrote the manuscript under the guidance of XP. XC, SW and TF performed the calculations and analyzed the results. XY participated in the discussions and provided valuable suggestions. All authors read and approved the final manuscript.

Availability of data and materials
The datasets used or analyzed during the current study are available from the corresponding authors on reasonable request.

Declarations

Competing interests
The authors declare that they have no competing interests.

Author details
[1] College of Mechanical Engineering, Chongqing University, Chongqing 400044, China. [2] Department of Engineering Mechanics, Chongqing University, Chongqing 400044, China. [3] State Key Laboratory of Coal Mine Disaster Dynamics and Control, Chongqing University, Chongqing 400044, China.

References
1. Wei SY, Zhang LF, Zheng SJ, Wang XP, Wang JW (2019) Deformation-induced interfacial transition zone in Cu/V nanolamellar multilayers. Scripta Mater 159:104–108
2. Xiang MZ, Liao Y, Wang K, Lu G, Chen J (2018) Shock-induced plasticity in semi-coherent 111 Cu-Ni multilayers. Int J Plast 103:23–38
3. Zheng Y, Li Q, Zhang J, Ye H, Zhang H, Shen L (2017) Hetero interface and twin boundary mediated strengthening in nano-twinned Cu//Ag multilayered materials. Nanotechnology 28:415705
4. Wang J, Misra A (2011) An overview of interface-dominated deformation mechanisms in metallic multilayers. Curr Opin Solid State Mater Sci 15:20–28
5. Fu T, Peng X, Chen X, Weng S, Hu N, Li Q, Wang Z (2016) Molecular dynamics simulation of nanoindentation on Cu/Ni nanotwinned multilayer films using a spherical indenter. Sci Rep 6:35665
6. Weng S, Ning H, Fu T, Hu N, Zhao Y, Huang C, Peng X (2018) Molecular dynamics study of strengthening mechanism of nanolaminated graphene/Cu composites under compression. Sci Rep 8:3089
7. Weng SY, Ning HM, Hu N, Yan C, Fu T, Peng XH, Fu SY, Zhang JY, Xu CH, Sun DY, Liu YL, Wu LK (2016) Strengthening effects of twin interface in Cu/Ni multilayer thin films—a molecular dynamics study. Mater Des 111:1–8
8. Yang WMC, Tsakalakos T, Hilliard JE (1977) Enhanced elastic-modulus in composition-modulated gold–nickel and copper–palladium foils. J Appl Phys 48:876–879
9. Davis BM, Seidman DN, Moreau A, Ketterson JB, Mattson J, Grimsditch M (1991) "Supermodulus effect" in Cu/Pd and Cu/Ni superlattices. Phys Rev B Condens Matter 43:9304–9307
10. Davis BM, Li DX, Seidman DN, Ketterson JB, Bhadra R, Grimsditch M (1992) Elastic and nanostructural properties of Cu/Pd superlattices. J Mater Res 7:1356–1369
11. Nasim M, Li YC, Wen M, Wen CE (2020) A review of high-strength nanolaminates and evaluation of their properties. J Mater Sci Technol 50:215–244
12. Howe CJ, Cropper MD, Fleming TP, Wardle RM, Bailey P, Noakes TCQ (2010) Ultra-thin films and surface alloying of Pd on Cu(111) investigated by medium energy ion scattering. Surf Sci 604:201–209
13. Weng S, Chen X, Yue X, Fu T, Peng X (2019) Inapparent strengthening effect of twin interface in Cu/Pd multilayered films with a large lattice mismatch. Nanomaterials 9:1778
14. Shao S, Akasheh F, Wang J, Liu Y (2018) Alternative misfit dislocations pattern in semi-coherent FCC 100 interfaces. Acta Mater 144:177–186
15. Shao S, Wang J (2015) Relaxation mechanisms, structure and properties of semi-coherent interfaces. Metals 5:1887–1901
16. Shao S, Wang J (2016) Relaxation, structure, and properties of semicoherent interfaces. JOM 68:242–252
17. Shao S, Wang J, Beyerlein IJ, Misra A (2015) Glide dislocation nucleation from dislocation nodes at semi-coherent 111 Cu–Ni interfaces. Acta Mater 98:206–220
18. An M, Deng Q, Li Y, Song H, Su M, Cai J (2017) Molecular dynamics study of tension-compression asymmetry of nanocrystal α-Ti with stacking fault. Mater Des 127:204–214
19. An MR, Deng Q, Su MJ, Song HY, Li YL (2017) Dependence of deformation mechanisms on layer spacing in multilayered Ti/Al composite. Mater Sci Eng A-Struct Mater Prop Microstruct Process 684:491–499
20. Zhou H, Li X, Qu S, Yang W, Gao H (2014) A jogged dislocation governed strengthening mechanism in nanotwinned metals. Nano Lett 14:5075–5080
21. Zhu YX, Li ZH, Huang MS, Liu Y (2015) Strengthening mechanisms of the nanolayered polycrystalline metallic multilayers assisted by twins. Int J Plast 72:168–184
22. Weng S, Ning H, Fu T, Hu N, Wang S, Huang K, Peng X, Qi HJ, Yan C (2019) Anisotropic and asymmetric deformation mechanisms of nanolaminated graphene/Cu composites. Nano Mater Sci 1:121–130
23. Weng S, Fu T, Peng X, Chen X (2019) Anisotropic phase transformation in B2 crystalline CuZr alloy. Nanoscale Res Lett 14:283
24. Fu T, Peng XH, Huang C, Zhao YB, Weng SY, Chen X, Hu N (2017) Effects of twin boundaries in vanadium nitride films subjected to tensile/compressive deformations. Appl Surf Sci 426:262–270
25. Weng S, Chen X, Yue X, Fu T, Peng X (2019) Inapparent strengthening effect of twin interface in Cu/Pd multilayered films with a large lattice mismatch. Nanomaterials (Basel) 9:1778
26. Fu T, Peng X, Feng C, Zhao Y, Wang Z (2015) MD simulation of growth of Pd on Cu (1 1 1) and Cu on Pd (1 1 1) substrates. Appl Surf Sci 356:651–658
27. Kunz MR, Mcclain SM, Chen DP, Koczkur KM, Weiner RG, Skrabalak SE (2017) Seed-mediated co-reduction in a large lattice mismatch system: synthesis of Pd-Cu nanostructures. Nanoscale 9:7570–7576
28. Wei W, Liu LC, Gong HR, Song M, Chang ML, Chen DC (2019) Fundamental mechanism of BCC-FCC phase transition from a constructed PdCu potential through molecular dynamics simulation. Comput Mater Sci 159:440–447
29. Baskes MI (1987) Application of the embedded-atom method to covalent materials: a semiempirical potential for silicon. Phys Rev Lett 59:2666–2669
30. Lee BJ, Baskes MI (2000) Second nearest-neighbor modified embedded-atom-method potential. Phys Rev B 62:8564–8567
31. Lee BJ, Shim JH, Baskes MI (2003) Semiempirical atomic potentials for the fcc metals Cu, Ag, Au, Ni, Pd, Pt, Al, and Pb based on first and second nearest-neighbor modified embedded atom method. Phys Rev B 68:144112
32. Liu Y, Bufford D, Rios S, Wang H, Chen J, Zhang JY, Zhang X (2012) A formation mechanism for ultra-thin nanotwins in highly textured Cu/Ni multilayers. J Appl Phys 111:073526
33. Liu Y, Bufford D, Wang H, Sun C, Zhang X (2011) Mechanical properties of highly textured Cu/Ni multilayers. Acta Mater 59:1924–1933
34. Hoover WG (1985) Canonical dynamics: equilibrium phase-space distributions. Phys Rev A 31:1695–1697
35. Hoover WG (1986) Constant-pressure equations of motion. Phys Rev A 34:2499–2500
36. Plimpton S (1995) Fast parallel algorithms for short-range molecular-dynamics. J Comput Phys 117:1–19

Chen *et al. Nanoscale Res Lett*   *(2021) 16:69*

Page 10 of 10

37. Stukowski A, Bulatov VV, Arsenlis A (2012) Automated identification and indexing of dislocations in crystal interfaces. Modell Simul Mater Sci Eng 20:085007
38. Stukowski A (2012) Structure identification methods for atomistic simulations of crystalline materials. Modell Simul Mater Sci Eng 20:045021
39. Zhao YB, Peng XH, Fu T, Sun R, Feng C, Wang ZC (2015) MD simulation of nanoindentation on (001) and (111) surfaces of Ag-Ni multilayers. Phys E 74:481–488
40. Shao S, Wang J, Misra A (2014) Energy minimization mechanisms of semi-coherent interfaces. J Appl Phys 116:023508
41. Shao S, Wang J, Misra A, Hoagland RG (2013) Spiral patterns of dislocations at nodes in (111) semi-coherent FCC interfaces. Sci Rep 3:2448
42. Huang CX, Wang YF, Ma XL, Yin S, Hoppel HW, Goken M, Wu XL, Gao HJ, Zhu YT (2018) Interface affected zone for optimal strength and ductility in heterogeneous laminate. Mater Today 21:713–719
43. Wu LP, Yu WS, Hu SL, Shen SP (2018) Radiation response of nanotwinned Cu under multiple-collision cascades. J Nucl Mater 505:183–192
44. Wu LP, Yu WS, Hu SL, Shen SP (2018) Size-dependent stability of stacking fault tetrahedron in coherent twin boundary bicrystal: Comparisons among Al, Ni, Cu and Ag. Comput Mater Sci 155:256–265
45. Fu T, Peng XH, Huang C, Yin DQ, Li QB, Wang ZC (2015) Molecular dynamics simulation of VN thin films under indentation. Appl Surf Sci 357:643–650
46. Sun S, Peng XH, Xiang HG, Huang C, Yang B, Gao FS, Fu T (2017) Molecular dynamics simulation in single crystal 3C-SiC under nanoindentation: formation of prismatic loops. Ceram Int 43:16313–16318

Publisher's Note

Springer Nature remains neutral with regard to jurisdictional claims in published maps and institutional affiliations.